

Numerical predictions of oblique detonation stability boundaries

M. J. Grismer¹, J. M. Powers²

¹ Computational Aerodynamics Engineer, WL/FIMC Bldg. 450, 2645 Fifth St. Ste. 7, Wright-Patterson AFB, Ohio 45433-7913, USA

² Associate Professor, Dept. of Aerospace and Mechanical Engineering, University of Notre Dame, Notre Dame, Indiana 46556-5637, USA

Received 4 August 1996 / Accepted 5 March 1996

Abstract. Oblique detonation stability was studied by numerically integrating the two-dimensional, one-step reactive Euler equations in a generalized, curvilinear coordinate system. The integration was accomplished using the Roe scheme combined with fractional stepping; nonlinear flux limiting was used to prevent unphysical solution oscillations near discontinuities. The method was verified on one- and two-dimensional flows with exact solutions, and its ability to correctly predict one-dimensional detonation stability boundaries was demonstrated. The behavior of straight oblique detonations attached to curved walls was then considered. Using the exact, steady oblique detonation solution as an initial condition, the numerical simulation predicted both steady and unsteady oblique detonation solutions when a detonation parameter known as the normal overdrive, f_n , was varied. For a standard test case with a specific heat ratio of $\gamma = 1.2$, a dimensionless activation energy of $\Theta = 50$, and dimensionless heat release of $q = 50$, an oblique detonation with a constant dimensionless component of velocity tangent to the lead shock, $v_{\tan} = 4.795$, underwent transition to unstable behavior at $f_n = 1.77$. This is slightly higher than the threshold of $f_n = 1.73$ predicted by one-dimensional theory; thus, the two-dimensionality renders the flow slightly more susceptible to instability.

Key words: Oblique detonation, Shock-induced combustion, Detonation instability

1 Introduction

High-speed nonequilibrium flows have been receiving more attention in recent years due to renewed interest in hypersonic air- and spacecraft such as the (now defunct) National Aerospace Plane (NASP) and the recent NASA/industry sponsored X-33 reusable launch vehicle demonstrator program. These vehicles may require novel propulsion devices, such as

the high-speed scramjets being studied by the Air Force Hypersonic System Technology Program (HySTP). The oblique detonation wave engine (ODWE) is another concept for high-speed propulsion. It relies upon oblique detonations to ignite a fuel-air mixture supersonically and thus provide thrust (Dunlap and Brehm 1958). The ram accelerator also utilizes oblique detonations to provide thrust, in this case to accelerate small projectiles to very high speeds (Hertzberg et al. 1988; Yungster and Bruckner 1992; Grismer and Powers 1995).

In order to optimize the performance of devices such as the ODWE and ram accelerator, it is important to gain a fundamental understanding of oblique detonation behavior. Experimental (Ruegg and Dorsey 1962; Lehr 1972) and numerical (Fickett and Wood 1966; Bourlioux et al. 1991) studies of fundamentally one-dimensional detonations with resolved reaction zone structure, the type originally studied independently by Zeldovich, von Neumann, and Doering (ZND), have shown that under certain conditions ZND detonations have an unsteady, oscillating character, while under other conditions they are stable. In the unsteady regime, peak flow quantities (such as pressure, density, or velocity) following the detonation can vary greatly from their average values. Similar phenomena occur in multiple dimensions (Fickett and Davis 1979). Very recently, new experimental evidence of oblique detonations over a wedge was presented (Morris et al. 1995). As a first step in understanding oblique detonation behavior, it is important to understand the relation between one-dimensional detonation instability and oblique detonation instability and to understand the behavior of oblique detonations in the unstable regime. This study focuses on extending one-dimensional stability results to two-dimensions for a simple model problem.

The stability of one-dimensional (ZND) detonations has been studied both analytically, using linearized equations, and numerically, using the complete, nonlinear equations. Fickett and Davis (1979) present a summary of the limited linear analytical stability results available in 1979, mostly attributable to Erpenbeck, cf. Erpenbeck (1969). Lee and Stewart (1990) performed a linear analysis of the stability of ZND detonations to longitudinal disturbances. They were able to both support the results of the previous studies, and then fill in and extend the range of parameters (activation energy, heat release, longitudinal wave number) which determine stability boundaries.

Correspondence to: M.J. Grismer;
 e-mail: grismemj@fim.wpafb.af.mil

This paper was presented at the 15th International Colloquium on the Dynamics of Explosions and Reactive Systems, Boulder, Colorado, USA, July 30–August 4, 1995

One of the results of these analyses was that for given values of heat release and activation energy, stability could often be achieved by increasing the level of overdrive. Here overdrive, to be precisely defined later, is used in the context of the classical piston-problem in which a piston is driven into a combustible mixture so as to induce a detonation. As the driving piston speed is increased, the overdrive is said to increase.

In brief, the theory which has emerged from these studies for detonation instability near the stability limit is as follows. A detonation instability can result from a perturbation in pressure in the interior of the reaction zone. The local compression gives rise to a local temperature increase with a consequent increase in the local reaction rate. This increases the magnitude of the compression and accelerates it toward the shock. The shock pressure peaks when the internal compression reaches it, resulting in flow variables in the reaction zone having gradients steeper than those which occur at steady state. The shock pressure then begins to drop as the chemical reaction is unable to maintain these high gradients, and is further lowered as the rarefaction resulting from and following the compression overtakes the shock. The cycle then repeats. In multiple dimensions the slightest asymmetry in the initial pressure perturbation, resulting from slight variations in the pre-shocked state, for example, lead to an asymmetry in the developing longitudinal instability. This in turn results in a transverse instability in which the detonation front deforms into multiple, curved cellular regions, and the reaction zone becomes a complex region of interacting reflected shocks and pockets of intense reaction.

Time-accurate numerical studies of ZND detonations have been performed to verify the linear stability analyses and to determine the nonlinear behavior of the detonation. Fickett and Wood (1966) used the method of characteristics to find pulsating detonations that were consistent with the linearized stability results. The unstable detonations oscillated about the steady solution, with peak pressures approximately fifty percent higher than the steady pressure. Later, Bourlioux, Majda, and Roytburd (1991) studied unstable detonations and made detailed comparisons to the results of Lee and Stewart (1990). Using an asymptotic analysis, they were able to show that their numerical method was predicting the correct unstable behavior. Then Bourlioux and Majda (1992) extended the study to two spatial dimensions, finding complex two-dimensional cellular structures arising from the original one-dimensional, steady detonation. Much of the recent work on unstable detonations is summarized in the review article of Bourlioux and Majda (1995).

The format of this article is as follows: the model equations considered in this study will be presented, followed by a description of the numerical method used to solve them. Next the numerical and physical boundary conditions used in the study will be described, and the results of a number of verification studies presented. This will be followed by a description of the methodology used to ascertain oblique detonation stability characteristics and the results of the numerical study. Final remarks regarding the results will then be made.

2 Model equations

The model equations used in this study are the reactive Euler equations for a calorically perfect ideal gas with an irreversible, one-step exothermic chemical reaction governed by Arrhenius kinetics. These equations are a subset of equations that model more complex physics, and are the most basic system to be studied before more complex systems are considered. The equations are written next in a vector conservative form for a two-dimensional Cartesian coordinate system. They represent conservation of mass, momenta, and energy, and evolution of the product mass fraction:

$$\frac{\partial \mathbf{q}}{\partial t} + \frac{\partial \mathbf{f}}{\partial x} + \frac{\partial \mathbf{g}}{\partial y} = \mathbf{w}, \quad (1)$$

where

$$\mathbf{q} = \begin{bmatrix} \rho \\ \rho u \\ \rho v \\ \rho E \\ \rho Y_2 \end{bmatrix}, \quad \mathbf{f} = \begin{bmatrix} \rho u \\ \rho u^2 + p \\ \rho uv \\ \rho u H \\ \rho u Y_2 \end{bmatrix}, \quad \mathbf{g} = \begin{bmatrix} \rho v \\ \rho uv \\ \rho v^2 + p \\ \rho v H \\ \rho v Y_2 \end{bmatrix},$$

$$\mathbf{w} = \begin{bmatrix} 0 \\ 0 \\ 0 \\ 0 \\ \rho(1 - Y_2)e^{-\Theta/\rho} \end{bmatrix}.$$

The dependent variables are the density ρ , the Cartesian velocities u and v , the total energy per unit mass $E = e + (u^2 + v^2)/2$, the total enthalpy per unit mass $H = E + p/\rho$, and the product mass fraction Y_2 . The internal energy $e = p/[\rho(\gamma - 1)] - Y_2 q$ contains a parameter q representing the heat released in the reaction. The independent variables are the Cartesian coordinates x and y , and the time t ; the remaining dimensionless parameters are the activation energy Θ and the ratio of specific heats γ . The equations have been nondimensionalized by characteristic freestream quantities as follows:

$$\rho = \frac{\tilde{\rho}}{\tilde{\rho}_0} \quad p = \frac{\tilde{p}}{\tilde{p}_0} \quad u = \frac{\tilde{u}}{\sqrt{\tilde{p}_0/\tilde{\rho}_0}} \quad v = \frac{\tilde{v}}{\sqrt{\tilde{p}_0/\tilde{\rho}_0}}$$

$$E = \frac{\tilde{E}\tilde{\rho}_0}{\tilde{p}_0} \quad H = \frac{\tilde{H}\tilde{\rho}_0}{\tilde{p}_0} \quad e = \frac{\tilde{e}\tilde{\rho}_0}{\tilde{p}_0} \quad q = \frac{\tilde{q}\tilde{\rho}_0}{\tilde{p}_0} \quad (2)$$

$$\Theta = \frac{\tilde{\Theta}\tilde{\rho}_0}{\tilde{p}_0} \quad x = \frac{\tilde{B}\tilde{x}}{\sqrt{\tilde{p}_0/\tilde{\rho}_0}} \quad y = \frac{\tilde{B}\tilde{y}}{\sqrt{\tilde{p}_0/\tilde{\rho}_0}} \quad t = \tilde{B}\tilde{t}$$

where \tilde{B} is the Arrhenius prefactor, “ $\tilde{}$ ” denotes a dimensional quantity, and the subscript 0 denotes a freestream quantity. Note that it is easily shown that \mathbf{f} , \mathbf{g} , and \mathbf{w} can be written explicitly in terms of \mathbf{q} ; this also holds for the transformed form of these variables which are discussed next.

In order to consider complex geometries, these equations were transformed to a generalized, curvilinear coordinate system, $(x, y, t) \rightarrow (\xi, \eta, \tau)$, in such a manner so as to maintain their conservative form:

$$\frac{\partial \hat{\mathbf{q}}}{\partial \tau} + \frac{\partial \hat{\mathbf{f}}}{\partial \xi} + \frac{\partial \hat{\mathbf{g}}}{\partial \eta} = \hat{\mathbf{w}}, \quad (3)$$

where

$$\hat{\mathbf{q}} = \mathbf{q}/J = J^{-1} \begin{bmatrix} \rho \\ \rho u \\ \rho v \\ \rho E \\ \rho Y_2 \end{bmatrix},$$

$$\hat{\mathbf{f}} = (\xi_t \mathbf{q} + \xi_x \mathbf{f} + \xi_y \mathbf{g})/J = J^{-1} \begin{bmatrix} \rho U^c \\ \rho u U^c + \xi_x p \\ \rho v U^c + \xi_y p \\ \rho H U^c - \xi_t p \\ \rho Y_2 U^c \end{bmatrix},$$

$$\hat{\mathbf{g}} = (\eta_t \mathbf{q} + \eta_x \mathbf{f} + \eta_y \mathbf{g})/J = J^{-1} \begin{bmatrix} \rho V^c \\ \rho u V^c + \eta_x p \\ \rho v V^c + \eta_y p \\ \rho H V^c - \eta_t p \\ \rho Y_2 V^c \end{bmatrix},$$

$$\hat{\mathbf{w}} = \mathbf{w}/J = J^{-1} \begin{bmatrix} 0 \\ 0 \\ 0 \\ 0 \\ \rho(1 - Y_2)e^{-\Theta\rho/p} \end{bmatrix},$$

where $\xi_x, \xi_y, \xi_t, \eta_x, \eta_y,$ and η_t are grid metrics; $U^c = \xi_t + \xi_x u + \xi_y v$ and $V^c = \eta_t + \eta_x u + \eta_y v$ are the contravariant velocities, and $J = 1/(x_\xi y_\eta - y_\xi x_\eta)$ is the grid Jacobian. For this study the grid remained fixed; therefore, $\xi_t = \eta_t = 0$.

3 Numerical method

One of the main criteria for choosing the numerical algorithm in this study was that it be able to capture discontinuities cleanly without resorting to artificial dissipation methods. Artificial dissipation is undesirable because it could dampen physical oscillations in the unsteady solutions of interest. Godunov-based schemes are well equipped to satisfy this requirement. In particular, Roe (1981) showed that his approximate Riemann solution reduces to the standard Rankine-Hugoniot jump conditions for a shock discontinuity; thus it seemed well equipped to handle our problem. For this reason, and its successful application in the literature (Clarke et al. 1993), a Godunov scheme based upon Roe's approximate Riemann solver, also known as Roe's scheme, was chosen for this study.

The curvilinear model equations were solved using Roe's scheme extended to second-order spatial accuracy with linear flux extrapolation, and made total variation diminishing (TVD) using nonlinear limiting functions (Chakravarthy and Osher 1985). Fractional stepping was used to extend the method to two spatial dimensions, and also made it possible to integrate the product mass fraction equation analytically (Colella et al. 1986). Second-order temporal accuracy was achieved with a two-step Runge-Kutta time integration and the fractional stepping order suggested by Strang (1968). Thus, in smooth regions of the flow, the scheme is formally second-order accurate; near discontinuities the nonlinear flux limiting reduces

the spatial accuracy to first-order to eliminate nonphysical solution oscillations.

The algorithm, as reported in detail by Grismer (1994), is outlined as follows: the solution at cell i after two timesteps, $\tau^{n+2} = \tau^n + 2\Delta\tau$, is determined by

$$\hat{\mathbf{q}}_i^{n+2} = \mathcal{L}_\xi^{\Delta\tau} \mathcal{L}_\eta^{\Delta\tau} \mathcal{L}_Y^{\Delta\tau} \mathcal{L}_Y^{\Delta\tau} \mathcal{L}_\eta^{\Delta\tau} \mathcal{L}_\xi^{\Delta\tau} \hat{\mathbf{q}}_i^n, \quad (4)$$

where $\mathcal{L}_\xi^{\Delta\tau}$ and $\mathcal{L}_\eta^{\Delta\tau}$ are the solution operators over $\Delta\tau$ in the ξ and η directions, respectively, and $\mathcal{L}_Y^{\Delta\tau}$ is the solution operator for the mass fraction over $\Delta\tau$. The operation $\mathcal{L}_\xi^{\Delta\tau} \hat{\mathbf{q}}_i^n$ is

$$\hat{\mathbf{q}}_i^\dagger = \hat{\mathbf{q}}_i^n - \frac{\Delta\tau}{2\Delta\xi} (\bar{\mathbf{f}}_{i+1/2}^{(2)n} - \bar{\mathbf{f}}_{i-1/2}^{(2)n}), \quad (5)$$

$$\hat{\mathbf{q}}_i^{n+1} = \hat{\mathbf{q}}_i^n - \frac{\Delta\tau}{\Delta\xi} (\bar{\mathbf{f}}_{i+1/2}^{(2)\dagger} - \bar{\mathbf{f}}_{i-1/2}^{(2)\dagger}), \quad (6)$$

where $\bar{\mathbf{f}}^{(2)\dagger}$ is the second-order interface flux determined from the half time step solution, $\hat{\mathbf{q}}^\dagger$. The second-order fluxes are determined with the following equations

$$\bar{\mathbf{f}}_{i+1/2}^{(2)} = \bar{\mathbf{f}}_{i+1/2} + \frac{1}{2} \left[\sum_{m=1}^N d\check{\mathbf{f}}_{i-1/2}^{m+} - \sum_{m=1}^N d\check{\mathbf{f}}_{i+3/2}^{m-} \right], \quad (7)$$

where

$$\bar{\mathbf{f}}_{i+1/2} = \frac{1}{2} (\hat{\mathbf{f}}_i + \hat{\mathbf{f}}_{i+1}) - \frac{1}{2} \sum_{m=1}^N (\alpha_m |\bar{\lambda}_m| \bar{\mathbf{f}}_m)_{i+1/2}, \quad (8)$$

is Roe's first-order flux,

$$d\check{\mathbf{f}}_{i-1/2}^{m+} = \check{\sigma}_{i-1/2}^{m+} (\bar{\mathbf{f}}_m)_{i+1/2}, \quad (9)$$

$$d\check{\mathbf{f}}_{i+3/2}^{m-} = \check{\sigma}_{i+3/2}^{m-} (\bar{\mathbf{f}}_m)_{i+1/2}, \quad (10)$$

are the limited flux increments, and

$$\check{\sigma}_{i-1/2}^{m+} = L[(\alpha_m \bar{\lambda}_{m+})_{i-1/2}, (\alpha_m \bar{\lambda}_{m+})_{i+1/2}], \quad (11)$$

$$\check{\sigma}_{i+3/2}^{m-} = L[(\alpha_m \bar{\lambda}_{m-})_{i+3/2}, (\alpha_m \bar{\lambda}_{m-})_{i+1/2}]. \quad (12)$$

In the above equations $\hat{\mathbf{f}}_i$ is the flux at cell-center i , N is the number of scalar equations in Eq. 3 (here $N = 5$), $\bar{\lambda}_m$ and $\bar{\mathbf{f}}_m$ are the m^{th} eigenvalue and right eigenvector of the Roe averaged version of the flux Jacobian matrix $\hat{\mathbf{A}} = \partial\hat{\mathbf{f}}/\partial\hat{\mathbf{q}}$, $\bar{\lambda}_{m+}$ and $\bar{\lambda}_{m-}$ indicate the respective positive and negative eigenvalues only, L indicates a nonlinear limiting function, and α_m is determined from $\alpha = \bar{\mathbf{R}}^{-1}(\hat{\mathbf{q}}_{i+1} - \hat{\mathbf{q}}_i)$ (where $\bar{\mathbf{R}}$ is the matrix of right eigenvectors). The choice of the limiting function is not unique; van Leer's limiter was chosen for this study and is defined as

$$L[a, b] = \frac{ab + |ab|}{a + b}. \quad (13)$$

$\mathcal{L}_\eta^{\Delta\tau} \hat{\mathbf{q}}_i^n$ is determined from equations of the same form as above, except that \mathbf{f} is replaced by \mathbf{g} , the eigenvalues and eigenvectors are determined from the Roe averaged version of the flux Jacobian matrix $\hat{\mathbf{B}} = \partial\hat{\mathbf{g}}/\partial\hat{\mathbf{q}}$, and $\Delta\xi$ is replaced by $\Delta\eta$.

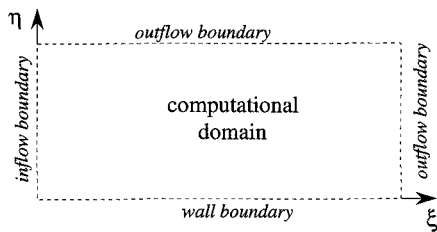


Fig. 1. Types of conditions required for computational domain boundaries

Lastly, the analytic integration of the species equations results in the operation $\mathcal{L}_Y^{\Delta\tau} \hat{q}_i^n$ being

$$Y_2^{n+1} = 1 + (Y_2^n - 1)e^{-\Delta\tau \exp(-\Theta\rho^n/p^n)}, \quad (14)$$

while all other variables remain constant.

Since Roe's approximate Riemann solver does not account for the interaction of multiple Riemann problems, the maximum time step for the scheme is determined by the time it takes the fastest wave in the domain to cross half of a computational cell. The fastest wave corresponds to the largest eigenvalue $\bar{\lambda}$, which leads to the following CFL criteria

$$\text{CFL} = \frac{\max(\bar{\lambda})\Delta\tau}{\Delta\xi} = 0.5. \quad (15)$$

A more conservative estimate of $\text{CFL} = 0.35\text{--}0.40$ was used in the numerical studies.

Figure 1 indicates the types of boundary conditions required for the various boundaries of the computational domain. The flow was considered to be entering the domain from the left at the inflow boundary, and exiting to the right at the outflow boundary. The incoming flow was always supersonic, while the outgoing flow could be either supersonic or subsonic. An impenetrable wall was modelled along the bottom of the domain, while the top of the domain was also treated as an outflow boundary.

An approach for handling inflow and outflow boundary conditions was adopted based on the characteristics of the one-dimensional form of the governing equations (Poinsot and Lele 1992). The sign of the characteristics of the equations in the coordinate direction crossing the boundary determine the direction in which information is physically propagating. For example, at the inflow boundary positive characteristics indicate that information is propagating into the domain, while negative characteristics indicate information is propagating out of the domain. Therefore, the boundary conditions that are used must adhere to this physical mechanism. The inflow boundary is straightforward: all characteristics are positive for supersonic inflow; therefore, information is only propagating into the domain. Numerically, this requires that all of the flow variables be specified at the inflow boundary.

The right outflow boundary is less trivial. For a supersonic outflow, all characteristics point out of the domain, while for a subsonic outflow four characteristics point out and one points in. Physically this means that information is only propagating out of the domain in a supersonic outflow, but both out

of and into the domain for a subsonic outflow. Numerically, a supersonic outflow requires that the variables at the outflow boundary be entirely specified using quantities from within the domain. The numerical condition for a subsonic outflow is difficult, however, because it requires information from outside the domain that is unknown (at least for the cases studied in this research). Following Thompson (1987) the conservation equations were transformed to a characteristic form in which variable quantities were associated with each of the characteristics. Those quantities associated with outgoing characteristics were computed from values interior to the domain, while the quantity associated with the incoming characteristic was estimated by the following simple term, $K(p_b - p_0)$ (Poinsot and Lele 1992), where K is a constant, p_0 is the freestream pressure, and p_b is the pressure at the subsonic boundary. Inert oblique shock simulations were used to estimate a value of $K = 0.025$ (Grismer 1994). Finally, slip conditions were used at the wall boundary, with the wall pressure estimated using one-dimensional Riemann invariants (Dadone and Grossman 1992).

4 Verification studies

The numerical algorithm was verified on the following test problems (Grismer 1994): the inert Riemann problem, steady and unsteady ZND detonations, inert supersonic flow over a wedge, and the straight wall, curved oblique detonation problem of Powers and Stewart (1992). Of the four test cases considered, only the unsteady ZND detonation has no known analytical solution; it has been studied extensively in the literature (Fickett and Wood 1966; Bourlioux et al. 1991), however, so detailed numerical solutions are available.

Figure 2 shows a comparison of the first- and second-order Roe scheme density solutions with the exact inert Riemann solution for an initial pressure ratio of 10, an initial density ratio of 8, an initial velocity of zero, $q = 0$, and $\gamma = 1.4$. The numerical solutions were on an equally spaced grid of 200 points, and the quantities have been scaled by their maximum values. Both numerical solutions capture the expansion, contact discontinuity, and shock; the second-order solution shows an improvement in quality over the first-order solution. The other flow variables showed similar improvement. It was shown (Grismer 1994) that the numerical solution converged to the exact solution with a calculated order of accuracy of 0.71 for the nominally first-order scheme and 0.99 for the nominally second-order scheme. This type of behavior was noted previously by Woodward and Colella (1984), who considered various schemes applied to one-dimensional, nonlinear problems.

Figure 3 shows the numerical unsteady peak pressure solution obtained for a one-dimensional detonation with $f = 1.6$, $\Theta = 50$, $q = 50$, and $\gamma = 1.2$. This detonation is known to be unstable (Lee and Stewart 1990). Here, f is the overdrive factor defined as $f = (D/D_{CJ})^2$, where D and D_{CJ} are defined from steady state theory: D is the wavespeed which is predicted by an *a priori* steady model of a piston driving a detonation into a combustible gas; D_{CJ} is the Chapman-Jouguet

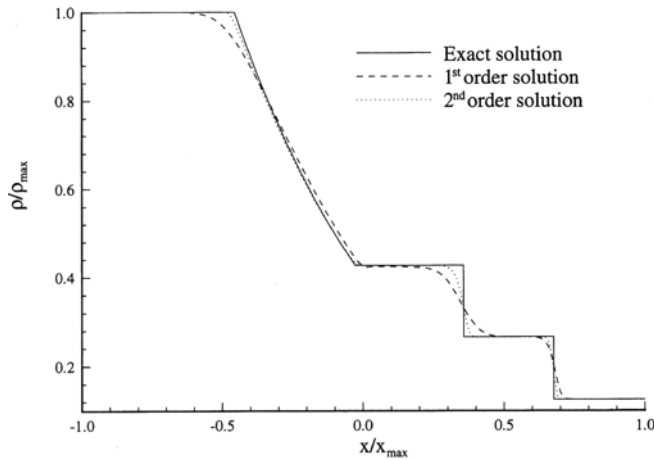


Fig. 2. Comparison of Roe scheme solutions with exact density solution of inert Riemann problem (initial pressure ratio = 10, density ratio = 8, quiescent conditions, $q = 0$, $\gamma = 1.4$)

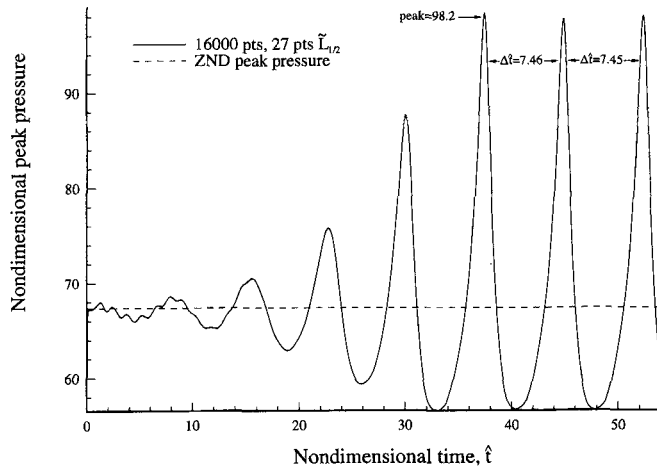


Fig. 3. Unsteady ZND detonation peak pressures ($f = 1.6$, $\Theta = 50$, $q = 50$, $\gamma = 1.2$)

(CJ) velocity predicted by steady theory for an unsupported detonation in the same gas; $D \geq D_{CJ}$. The time scale shown in Fig. 3 has been rescaled from Eq. 2 in order to directly compare to the results of Bourlioux, et al. (1991). Here we define $\hat{t} = (\tilde{t} \sqrt{\tilde{p}_0 / \tilde{\rho}_0}) / \tilde{L}_{1/2}$ where $\tilde{L}_{1/2}$ is also defined from an *a priori* steady theory to be the distance from the lead shock to the point in the reaction zone at which the reaction is half complete, $\lambda = 1/2$. The maximum peak pressures and periods of oscillation show good agreement with Bourlioux et al. (1991). Furthermore, numerical simulations for cases in which the detonations were known to be stable resulted in the correct steady solutions. The numerically determined stability boundary of 1.73 ± 0.01 agreed very well with the linear analysis result of 1.73; further accuracy could have been achieved with the numerical method, but was not attempted.

Figure 4 shows pressure contours from the numerical solution obtained for inert, supersonic flow over a wedge of half angle $\theta = 20^\circ$ and with $\gamma = 1.4$, $\mathcal{M}_{x0} = 4$, and $q = 0$. Here, \mathcal{M}_{x0} is the freestream Mach number defined

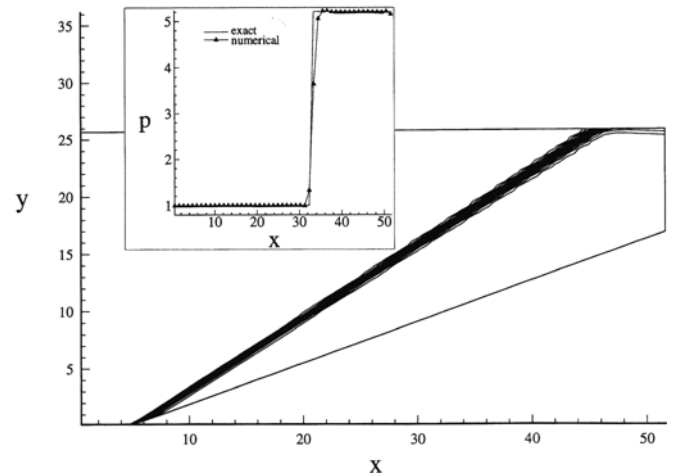


Fig. 4. Pressure contours for supersonic flow over a wedge ($\mathcal{M}_0 = 4$, $\theta = 20^\circ$, $\gamma = 1.4$, $q = 0$). Inset: Comparison of numerical and exact solution along $\eta = \text{constant}$ interior grid line

as $\mathcal{M}_{x0} = \tilde{u}_0 / \sqrt{\gamma \tilde{p}_0 / \tilde{\rho}_0}$. This case was a test of the outflow condition along the top of the domain; in particular the one-dimensional characteristic analysis indicates that one unknown characteristic is entering the domain. Thus, the incoming wave was estimated as discussed previously. It is apparent that there is still some reflection of the shock at the top boundary. However, both the shock angle, and the shocked flow quantities in the region behind the shock and away from the top boundary (see Fig. 4 inset), agree well with the exact solution.

Finally, in a comparison similar to that done by Grismer and Powers (1992) using NASA Lewis' RPLUS code, the present code's predictions were compared to the asymptotic solution of Powers and Stewart (1992). Figures 5 and 6 show numerical and asymptotic pressure solutions for an oblique detonation over a $\theta = 20^\circ$ wedge with $\mathcal{M}_{x0} = 20$, $q = 10$, $\gamma = 1.4$, and $\Theta = 0$. For the purposes of comparison, like contour values are indicated on each figure; note that the changes in pressure are rather small between contours. The same types of features are evident in each figure: a curved detonation front, and similar contour locations. Toward the rear of the domain, small oscillations degrade the numerical solution. A comparison of the wedge surface pressures between the two solutions showed very good agreement, except at the wedge apex where the numerical solution slightly overshoot the asymptotic solution (Grismer 1994). Overall, the numerical algorithm accurately predicted each of the solutions in the verification study.

5 Results

In order to make more direct comparisons with one-dimensional stability results, straight oblique detonations attached to curved walls were studied. The straight shock, curved wall detonation solution is simply the ZND detonation solution with an added constant transverse velocity component. The resulting flowfield following the detonation has curved streamlines, one of which can be interpreted as a curved wall. Since this

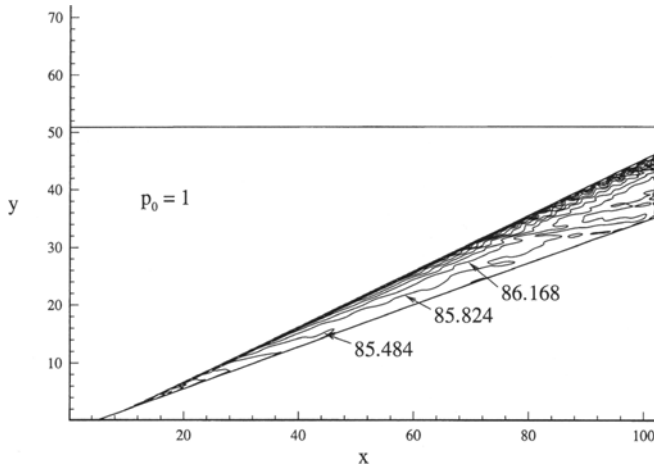


Fig. 5. Oblique detonation pressure contours for numerical solution ($\mathcal{M}_0 = 20$, $\theta = 20^\circ$, $q = 10$, $\gamma = 1.4$, $\Theta = 0$)

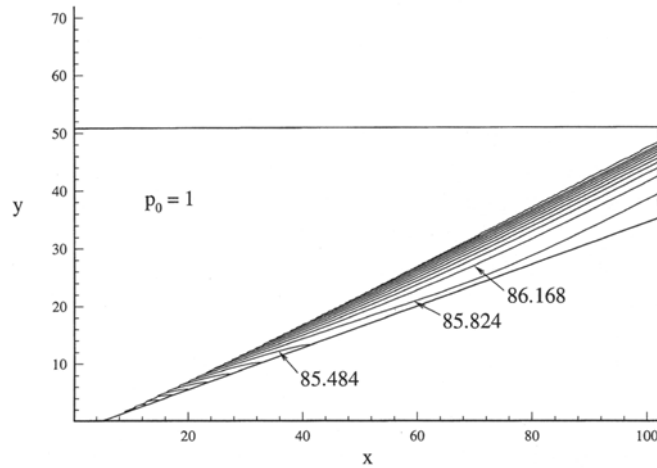


Fig. 6. Oblique detonation pressure contours for asymptotic solution ($\mathcal{M}_0 = 20$, $\theta = 20^\circ$, $q = 10$, $\gamma = 1.4$, $\Theta = 0$)

oblique detonation is a simple extension of the ZND detonation, it is expected that the two would have related stability characteristics. For this study the parameter varied was the normal overdrive, f_n , which is simply the overdrive associated with the ZND detonation to which the transverse velocity component was added.

The solution procedure used for each case was as follows. A steady weak overdriven oblique detonation was calculated through numerical solution of ordinary differential equations using the procedure given in detail by Powers and Gonthier (1992) and adapted slightly for the one-step kinetics of the present study. The weak overdriven oblique detonation is on the weak branch of the oblique detonation polar. Nearly all oblique detonations of this class have a total Mach number which is supersonic and a Mach number in the direction normal to the incident shock which is subsonic throughout the reaction zone. This analysis yielded a steady solution for the full flowfield and for the shape of the wall necessary to support a straight shock wave. From this wall shape a computational mesh was generated which had some grid clustering near the

wall. The steady solution was then written on the grid of cell centers. As indicated by previous numerical one-dimensional detonation studies (Bourlioux et al. 1991), as well as our own verification studies, there is a need to maximize the number of points within the reaction zone of the detonation in order to successfully capture detonation instability. For this reason, the grid was generated such that the oblique detonation would exit through the top of the domain and not the rear; in this way it was possible to increase grid resolution within the reaction zone of the detonation while minimizing the total number of points needed for the computation. An additional parameter used to size the computational grid was the ratio κ of the initial shock length within the domain, L_{sh} , to the initial half reaction zone length; $\kappa = L_{sh}/L_{1/2}$. The exact solution on the grid was then used as an initial condition for the simulation, which was run continuously until the solution had reached a steady state or could not continue. Steady state was typically achieved when the residuals of the flow variables had decreased by two to three orders of magnitude. During execution, data files were written every two hundred time steps to follow the time-dependent nature of the solution. Complete solutions required anywhere from several hours to several days to finish when run on an IBM RS/6000 Model 350 workstation.

In all of the cases studied, the following parameters were held constant: $\Theta = 50$, $q = 50$, and $\gamma = 1.2$. Additionally, the same constant tangential velocity of $v_{tan} = 4.795$ was used in all cases to generate the exact solution. Different levels of normal overdrive f_n were then achieved by varying the freestream Mach number \mathcal{M}_{x0} . The values of heat release, activation energy, and γ were chosen to match those used in the unsteady one-dimensional detonation; the tangential velocity was chosen so the exact detonation solutions would be weak and overdriven.

Cases with normal overdrive values of $f_n = 1.6, 1.7, 1.76, 1.78, 1.8$, and 2.0 were considered; both stable and unstable oblique detonations were found. The unstable solutions were characterized by the formation of one or more three-shock structures at the detonation front. These structures were predicted to move downward along the front, and eventually impact with the wedge surface. The passage of the three-shock resulted in a curved detonation front which propagated forward into the freestream until encountering the front computational boundary. The initial transient stages of the stable oblique detonations were also characterized by the three-shock structures; however, in those cases the disturbance would simply propagate out the top of the domain, and the detonation would return approximately to its initial steady state.

Figures 7 and 8 illustrate the behavior of a typical unstable and stable case, respectively, with time-series plots of the density solutions obtained for two different normal overdrive values ($f_n = 1.76$ and 1.8 , respectively). The plots are sequential, though not equally spaced, in time, with frame (a) being the earliest, and frame (f) the latest. The forward propagation of the unstable detonation front is apparently the result of the increase in the detonation velocity due to the instability. The unstable simulations were stopped when the detonation front encountered the front computational boundary. It is possible

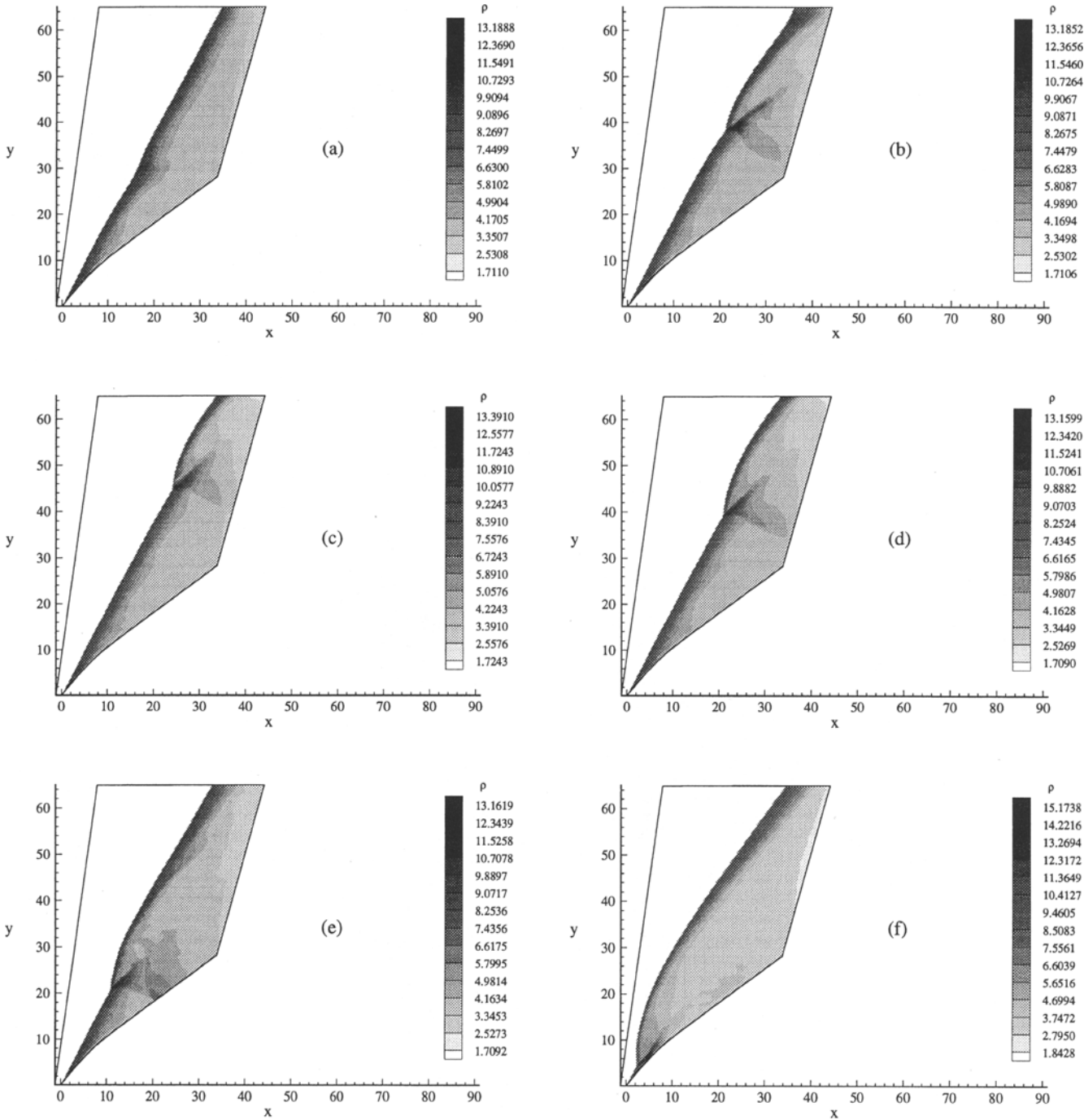


Fig. 7. Unstable oblique detonation shaded density contours as a function of time ($f_n = 1.76, \Theta = 50, q = 50, \gamma = 1.2$)

that given a large enough domain, the detonation would eventually weaken and return to the wedge, following the oscillatory cycle of the unstable ZND detonation.

It is apparent in the last frame of Fig. 8 that the final stable solution is not quite the exact steady solution; there are extraneous contours along the right and top boundary. These are reflections resulting from the approximate outflow boundary condition along the top of the domain. Figure 9 directly compares the final numerical solution to the exact steady solution by showing both sets of density contours. The contours coin-

cide well in the lower half of the plot, but in the upper half the numerical solution moves slightly in front of the exact solution. This is in contrast to the final steady numerical solution obtained for $f_n = 2.0$, which is compared to the exact solution in Fig. 10. In this case the numerical and exact solutions agree well, with only the upper right corner of the numerical solution indicating some reflection from the upper computational boundary. The transient portions of the two solutions were quite different; two three-shock structures formed and passed out of the domain at $f_n = 1.8$, while only one distur-

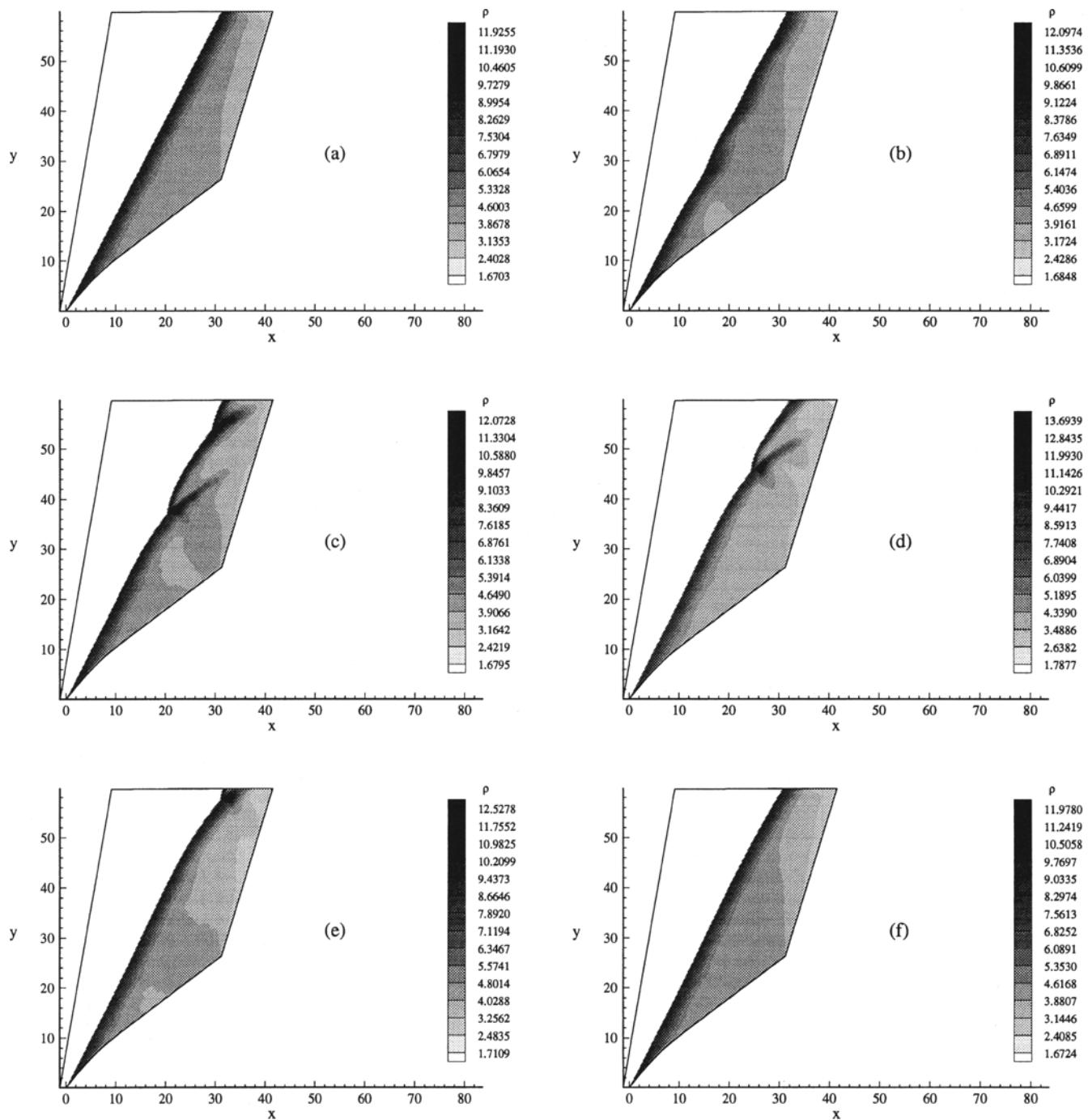


Fig. 8. Stable oblique detonation shaded density contours as a function of time ($f_n = 1.8$, $\Theta = 50$, $q = 50$, $\gamma = 1.2$)

bance began to coalesce and then passed out of the domain at $f_n = 2.0$ (see for example, the initial formation of the three-shock structures in frame (b) of Fig. 8). It is possible that the much larger initial variation in the solution at $f_n = 1.8$ resulted in the estimated outflow condition of Eq. 14 no longer being able to maintain the original steady solution, giving rise to somewhat larger discrepancies in the final steady solution. Another area of discrepancy between the numerical and exact solutions was along the wedge surface, particularly at the wedge apex. The numerical solutions for pressure and density

overshot the exact solution at the apex due to the discontinuity in the computational grid at this point, and in general the numerical solutions overestimated (or underestimated, depending upon the quantity) the exact solution near the wedge surface. Lastly, the final steady numerical solutions exhibited small oscillations following the detonation front. These were apparent in plots comparing the numerical and exact steady solutions along given $\eta = \text{constant}$ gridlines of the domain.

We next discuss the qualitative effects of resolution, as embodied in the number of points per $L_{1/2}$ and κ . For this

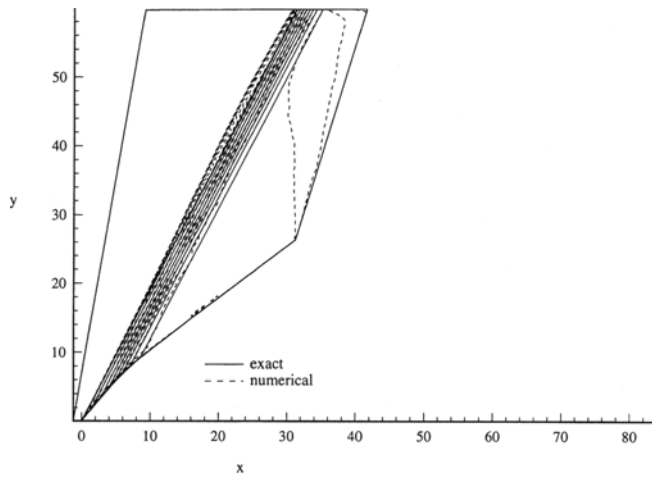


Fig. 9. Comparison of numerical and exact steady oblique detonation density contours ($f_n = 1.8$, $\Theta = 50$, $q = 50$, $\gamma = 1.2$)

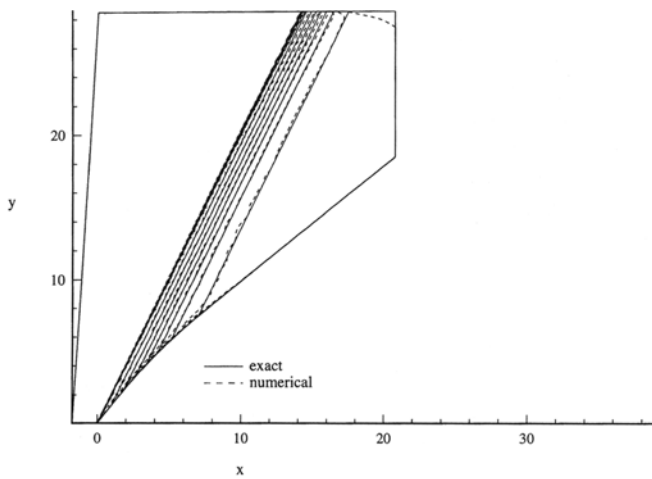


Fig. 10. Comparison of numerical and exact steady oblique detonation density contours ($f_n = 2.0$, $\Theta = 50$, $q = 50$, $\gamma = 1.2$)

numerical scheme the verification studies showed that as few as ten points per $L_{1/2}$ were sufficient to accurately predict the one-dimensional detonation instability. Not unexpectedly, this carried over to the oblique detonation studies, where at least this many points within the half reaction zone width was required to obtain a steady or unsteady solution that could withstand further grid refinement. Similarly, it was found that κ values of at least 20 were required for grid independent results. The distance between the two three-shock structures in frame *c* of Fig. 8, typically referred to as the cell size, is approximately $8L_{1/2}$. Thus the limiting value of κ found was enough to encompass two cells of this size in the detonation front. An expanded domain, impractical due to the finite available computational resources, would have likely yielded a larger number of cells such as those reported in the literature for channel flows.

Lastly it should be noted that the numerical modelling of reactive flows, even those with very simple chemistry models, is still an uncertain affair. Stewart and Bdzil (1993) note that

different, well-tested algorithms produced widely varying results for a model problem, even though the equations being solved were the relatively “simple” reactive Euler equations considered here.

6 Final remarks

The results obtained in the numerical study suggest that straight shock, curved wall oblique detonations have a stability threshold slightly higher than their one-dimensional counterparts. For the parameters studied, the oblique detonation stability threshold was at a normal overdrive value of $f_n = 1.77 \pm 0.01$, while the corresponding one-dimensional detonation threshold occurs at an overdrive of $f = 1.73$. The slightly higher stability threshold for the straight oblique detonation suggests that the initial “one-dimensional” instability, which decayed in one dimension, undergoes a transition to unstable two-dimensional structures for a small range of normal overdrive values. Above that range the two-dimensional structures that form are too weak to destabilize the detonation. It may be that further extending the top of the domain to increase κ past the values used could change the stability threshold observed. However, the instability in the solution at $f_n = 1.76$ occurred away from the upper boundary, so it is unlikely that the threshold would decrease. Finally, it is also possible that extending the computational domain horizontally to allow the curved detonation room to move forward could result in the eventual return of the detonation to a stable steady state.

As with any numerical study, particularly one involving the study of stability, there are a number of caveats concerning the above conclusions. Certainly the imperfect outflow condition along the top of the domain, and to a lesser extent the solid wall boundary condition near the wedge apex, may have affected the stability threshold prediction. Another issue is the unknown effect on the predicted detonation instability of the slight oscillations observed in the numerical solutions when compared to exact solutions. Certainly where issues of stability are concerned these are undesirable artifacts. Other researchers (Colella and Woodward 1984) have advocated adding very small amounts of artificial dissipation in higher-order Godunov schemes in order to eliminate such phenomena. This was avoided here due to the possible effects on the numerical prediction of instability. Without exact two-dimensional steady and unsteady solutions with which to compare, it is difficult to know which is the correct choice. A related issue is the nonunique choice of a limiter for the second order scheme. Which limiter is used will certainly affect the solution, but, as with artificial dissipation, the correct choice is not necessarily evident.

Acknowledgements. NASA Lewis Research Center, the Center for Applied Mathematics at the University of Notre Dame, the Department of Aerospace and Mechanical Engineering at the University of Notre Dame, and the Computational Fluid Dynamics Branch and Armaments Branch of Wright Laboratory all provided support at various stages of this research.

References

- Bourlioux A, Majda AJ (1992) Theoretical and numerical structure for unstable two-dimensional detonations. *Combust. Flame* 90:211
- Bourlioux A, Majda AJ (1995) Theoretical and numerical structure of unstable detonations. *Phil. Trans. R. Soc. Lond. A* 350:29
- Bourlioux A, Majda AJ, Roytburd V (1991) Theoretical and numerical structure for unstable one-dimensional detonations. *SIAM J. Appl. Math.* 51:303
- Chakravarthy SR, Osher S (1985) Computing with high-resolution upwind schemes for hyperbolic equations. In: Bjorn E. Enquist, Stanley Osher, Richard C.J. Somerville (eds) *Large-scale computations in fluid mechanics*. American Mathematical Society, Providence, pp 57–86
- Clarke JF, Karni S, Quirk JJ, Roe PL, Simmonds LG, Toro EF (1993) Numerical computation of two-dimensional unsteady detonation waves in high energy solids. *J. Comp. Phys.* 106:215
- Colella P, Majda AJ, Roytburd V (1986) Theoretical and numerical structure for reacting shock waves. *SIAM J. Sci. Stat. Comp.* 7:1059
- Colella P, Woodward PR (1984) The piecewise parabolic method (PPM) for gas-dynamical systems. *J. Comp. Phys.* 54:174
- Dadone A, Grossman B (1992) Characteristic-based, rotated upwind scheme for the Euler equations. *AIAA J.* 30:2219
- Dunlap R, Brehm RL (1958) A preliminary study of the application of steady-state detonative combustion to a reaction engine. *Jet Prop.* 28:451
- Erpenbeck JJ (1969) Theory of detonation stability. In: *Twelfth symposium (international) on combustion*. The Combustion Institute, New York, pp 711–721
- Fickett W, Davis WC (1979) *Detonation*. University of California Press, Berkeley Los Angeles London
- Fickett W, Wood WW (1966) Flow calculations for pulsating one-dimensional detonations. *Phys. Fluids* 9:903
- Grismer MJ, Powers JM (1992) Comparison of numerical oblique detonation solutions with an asymptotic benchmark. *AIAA J.* 30:2985
- Grismer MJ (1994) Numerical simulations of steady and unsteady oblique detonation phenomena with application to propulsion. PhD Dissertation, University of Notre Dame
- Grismer MJ, Powers JM (1995) Calculations for steady propagation of a generic ram accelerator configuration. *J. Prop. Power* 11:105
- Hertzberg A, Bruckner AP, Bogdanoff DW (1988) Ram accelerator: a new chemical method for accelerating projectiles to ultrahigh velocities. *AIAA J.* 26:195
- Hirsch C (1990) *Numerical computation of internal and external flows – vol. 2: computational methods for inviscid and viscous flows*. John Wiley & Sons, Chichester New York Brisbane Toronto Singapore
- Lee HI, Stewart DS (1990) Calculation of linear detonation instability: one-dimensional instability of plane detonation. *J. Fluid Mech.* 216:103
- Lehr HF (1972) Experiments on shock-induced combustion. *Astronautica Acta* 17:589
- Morris CI, Kamel M, Thurber MC, Wehe SD, Hanson RK (1995) Development of an expansion tube for investigation of combustion in supersonic projectile flowfields. *AIAA Paper* 95-2717
- Poinsot TJ, Lele SK (1992) Boundary conditions for direct simulations of compressible viscous flows. *J. Comp. Phys.* 101:104
- Powers JM, Gonthier KA (1992) Reaction zone structure for strong, weak overdriven, and weak underdriven oblique detonations. *Phys. Fluids A* 4:2082
- Powers JM, Stewart DS (1992) Approximate solutions for oblique detonations in the hypersonic limit. *AIAA J.* 30:726
- Roe PL (1981) Approximate Riemann solvers, parameter vectors, and difference schemes. *J. Comp. Phys.* 43:357
- Ruegg FW, Dorsey WW (1962) A missile technique for the study of detonation waves. *J. Res. National Bureau Standards-C Eng. Instrument.* 66C:51
- Stewart DS, Bdzil JB (1993) Asymptotics and multi-scale simulation in a numerical combustion laboratory. In: H. G. Kaper, M. Garbey (eds) *Asymptotic and numerical methods for partial differential equations with critical parameters*. Kluwer Academic Publishers, Boston
- Strang G (1968) On the construction and comparison of difference schemes. *SIAM J. Num. Anal.* 5:506
- Thompson KW (1987) Time dependent boundary conditions for hyperbolic systems. *J. Comp. Phys.* 68:1
- Woodward P and Colella P (1984) The numerical simulation of two-dimensional fluid flow with strong shocks. *J. Comp. Phys.* 54:115
- Yungster S, Bruckner AP (1992) Computational studies of a superdetonative ram accelerator mode. *J. Prop. Power.* 8:457